

Accretion, Ablation and Propeller Evolution in Close Millisecond Pulsar Binary Systems

Paul D. Kiel^{1, 2} • Ronald E. Taam^{1, 3}

Abstract A model for the formation and evolution of binary millisecond radio pulsars in systems with low mass companions ($< 0.1 M_{\odot}$) is investigated using a binary population synthesis technique. Taking into account the non conservative evolution of the system due to mass loss from an accretion disk as a result of propeller action and from the companion via ablation by the pulsar, the transition from the accretion powered to rotation powered phase is investigated. It is shown that the operation of the propeller and ablation mechanisms can be responsible for the formation and evolution of black widow millisecond pulsar systems from the low mass X-ray binary phase at an orbital period of ~ 0.1 day. For a range of population synthesis input parameters, the results reveal that a population of black widow millisecond pulsars characterized by orbital periods as long as ~ 0.4 days and companion masses as low as $\sim 0.005 M_{\odot}$ can be produced. The orbital periods and minimum companion mass of this radio millisecond pulsar population critically depend on the thermal bloating of the semi-degenerate hydrogen mass losing component, with longer orbital periods for a greater degree of bloating. Provided that the radius of the companion is increased by about a factor of 2 relative to a fully degenerate, zero temperature configuration, an approximate agreement between observed long orbital periods and theoretical modeling of hydrogen rich donors can be achieved. We find no discrepancy between the estimated birth rates for LMXBs and black

widow systems, which on average are $\sim 1.3 \times 10^{-5} \text{ yr}^{-1}$ and $1.3 \times 10^{-7} \text{ yr}^{-1}$ respectively.

Keywords binaries: close — magnetic fields — pulsars: general — pulsars: individual (PSR J1023+0038) — stars: neutron

1 Introduction

The discovery of a radio pulsar with a 1.69 ms spin period in J102347.67+003841.2 (Archibald et al. 2009), a system characterized by a 4.75 hr binary orbital period (Woudt et al. 2004), has provided observational confirmation of the link between rotation powered radio millisecond pulsars (MSPs) and the low mass X-ray binary (LMXB) phase. This source is of special interest since it appears to have undergone a transformation from a LMXB to a recycled MSP (see Bond et al. 2002; Thorstensen & Armstrong 2005; Wang et al. 2009). Takata, Cheng, & Taam (2010) suggested that the emission of γ -rays from the pulsar magnetosphere was important in facilitating the transformation of a MSP from the accretion powered to the rotation powered phase.

Among the binary MSPs, there is a class of systems characterized by short orbital periods (< 1 day), of which J102347.67+003841.2 is a member, from which we define two distinct populations. In one population, known as ultra compact binary X-ray MSPs (UCXBs), systems consist of MSP-white dwarf (WD) components with orbital periods $P_{\text{orb}} < 0.07$ days and companion masses, $M_c < 0.02 M_{\odot}$. The UCXB progenitors are thought to have experienced two common envelope (CE) phases, one initiated by the neutron star (NS) progenitor – while the companion was still on the main sequence (MS) – and the other initiated by a helium or carbon oxygen WD progenitor. The other population,

Paul D. Kiel

Ronald E. Taam

¹Center for Interdisciplinary Exploration and Research in Astrophysics (CIERA) and Dept. of Physics and Astronomy, Northwestern University, 2145 Sheridan Rd, Evanston, IL 60208

²Monash affiliate, Monash Centre for Astrophysics, Monash University, Victoria 3800, Australia

³Academia Sinica Institute of Astronomy and Astrophysics - TIARA, P.O. Box 23-141, Taipei, 10617 Taiwan

known as black widow binaries, is composed of a radio MSP and brown dwarf (partially degenerate MS star) with $0.1 < P_{\text{orb}} < 1.0$ days and $M_c < 0.07 M_{\odot}$. In contrast to the former population, these MSP binaries display regular eclipses of the pulsed signal over a portion of their orbit, providing direct evidence that the companion is undergoing ablation by the MSP. One of the primary differences between the black widow systems and the UCXB is related to the size of the companion star. As inferred from observations (King et al. 2005), the stellar radii of the companions are ~ 5 times smaller in UCXB systems, indicating that thermal bloating of the donor is important (Nelson & Rappaport 2003; King et al. 2005). Here, the donor refers to the star that is overflowing its Roche lobe. This difference in radii results in contrasting orbital periods, for the same companion mass, between these two populations.

In this paper we explore the evolution of a system from the LMXB phase to the binary MSP phase via a binary population synthesis technique taking into account the influence of propeller action in ejecting mass from an accretion disk and via ablation from the companion by a pulsar. Attention is focused on examining the long term orbital evolution of compact binary MSPs and black widow pulsars when including thermal bloating, ablation and propeller evolution into our models. In particular, we show that the transition from the LMXBs to black widow radio pulsars takes place when the models account for the propeller mechanism and ablation of the NS companion.

The population synthesis technique allows us to identify important and possibly interesting evolutionary scenarios and pathways in a simple manner – this is one of the goals of the work presented here. Hence, the population synthesis method is preferred over the use of a detailed code because it facilitates the modelling of many millions of different systems in exploring the influence of numerous assumptions and parameter values. Detailed codes, although more accurate in their physical output, require significantly greater computational expense.

In the next section, we outline the main assumptions for modeling accretion, ablation and propeller action in our population synthesis study and describe our method. The numerical results are presented and compared to detailed simulations in §3. Example outcomes for a range of systems are described in §4 with specific application to the black widow pulsar formation rates in §5. A discussion of our results is presented in §6, and we conclude in §7.

2 Formulation and Methodology

As mass loss from the system due to propeller action and/or from ablation of the companion plays an important role in the evolution considered here, the modeling of these effects is described below.

2.1 Modeling accretion, ablation and propeller physics

Mass transfer from one star to another greatly affects both the stellar components and the orbital evolution of the binary system. Here, we outline the main influence on the stellar components and orbit, focusing on the evolution of the stellar spins and the orbital angular momentum. Since the evolution during mass transfer depends upon the evolutionary phase of the system, we distinguish three regimes corresponding to the standard mass transfer, ablation, and propeller phases.

In the semi-detached phase, the amount of mass transferred, ΔM , mass accreted, ΔM_a , and mass lost from the system, ΔM_{lost} , is calculated according to Hurley, Tout & Pols (2002), where $\Delta M = \Delta M_{\text{lost}} + \Delta M_a$. If the mass transfer rate is greater than the Eddington rate, then $\Delta M_{\text{lost}} > 0$. The Eddington mass transfer rate, above which some mass is assumed lost from the system, is $\dot{M}_{\text{Edd}} = 2.08 \times 10^{-3} (1 + X) R_a M_{\odot} \text{ yr}^{-1}$, where $X = 0.76 - 3.0Z$ is the hydrogen abundance, Z is the metallicity and R_a is the neutron star radius in solar units. Note, subscript ‘a’ denotes accretor parameters (where the accretor is the NS), while subscript ‘d’ denotes donor star parameters (see below).

2.1.1 Standard RLOF evolution

We describe standard Roche lobe overflow (RLOF) evolution when the operation of the propeller or ablation mechanism (see below) is unimportant. The removal of ΔM from the donor modifies the donor’s spin which, in turn, is coupled to the orbit. Assuming that the system is in a steady state, the change in spin angular momentum is given by

$$(\Delta J_{\text{d spin}})_{\text{new}} = \Delta J_{\text{d spin}} - \Delta M R_{\text{d}}^2 \Omega_{\text{d}}, \quad (1)$$

and the change in orbital angular momentum by

$$(\Delta J_{\text{orb}})_{\text{new}} = \Delta J_{\text{orb}} + f_c \Delta M R_{\text{d}}^2 \Omega_{\text{d}}. \quad (2)$$

Here, R_{d} is the radius of the donor, Ω_{d} is its angular velocity and f_c is a coupling factor. $\Delta J_{\text{d spin}}$ and ΔJ_{orb} contain other evolutionary modifications to the donor spin and orbital angular momentum in the same time step as our modifications owing to mass transfer.

These additional adjustments are associated with tidal torques, magnetic braking (see Eqn. 20) and gravitational radiation (see Eqns. 21 and 22). The coupling factor indicates the amount of angular momentum that is introduced to the orbit. For simplicity we assume $f_c = 1$ unless otherwise stated. If the accretion rate onto the NS is super-Eddington, then

$$(\Delta J_{\text{orb}})_{\text{new}} = \Delta J_{\text{orb}} - \frac{\Delta M_{\text{lost}} M_{\text{d}}^2}{M_{\text{tot}}^2} a^2 \Omega_{\text{orb}} \sqrt{1 - e^2}, \quad (3)$$

where Ω_{orb} is the orbital angular velocity, e is the orbit eccentricity, a is the orbital separation, and $M_{\text{tot}} = M_{\text{a}} + M_{\text{d}}$ is the total mass of the system. The spin of the accretor is updated from

$$(\Delta J_{\text{a spin}})_{\text{new}} = \Delta J_{\text{a spin}} + \Delta M_{\text{a}} \sqrt{GM_{\text{a}} R_{\text{in}}}, \quad (4)$$

while the change in orbital angular momentum is updated by

$$(\Delta J_{\text{orb}})_{\text{new}} = \Delta J_{\text{orb}} - \Delta M_{\text{a}} \sqrt{M_{\text{a}} G R_{\text{in}}}. \quad (5)$$

The lever arm R_{in} is set equal to the larger of the neutron star radius or the magnetospheric radius, i.e., $R_{\text{in}} = \text{MAX}(R_{\text{a}}, R_{\text{m}})$, which is given as $R_{\text{m}} = 1.7 \times 10^{-4} R_{\odot} B_{\text{s}}^{4/7} R_{\text{NS}}^{12/7} M_{\text{NS}}^{-1/7} \dot{M}^{-2/7}$. Here, R_{m} is taken to be half of the Alfvén radius, which corresponds to the location where the magnetic field pressure equals the ram pressure of in falling material (Frank, King & Raine 2002). The pulsar magnetic field strength, B_{s} , is in units of Gauss, R_{NS} and M_{NS} are the pulsar radius and mass respectively in solar units, and \dot{M} is the mass transfer rate in $M_{\odot} \text{yr}^{-1}$.

2.1.2 Propeller, spin down and equilibrium spin down modes

The concept of propeller action operating in interacting binary systems was first suggested as a mechanism to facilitate mass loss in a pioneering study by Illarionov & Sunyaev (1975). Such an evolution requires a NS with a sufficiently strong magnetic field and sufficient rotation, at the magnetospheric boundary, to halt accretion and eject material from the inner edge of the accretion disk. In this process, the propeller mechanism expels incoming material at the expense of the NS's angular momentum. During this phase the NS spin angular momentum and orbital angular momentum are updated as described by Kiel et al. (2008) and outlined below.

In this case, the donor spins down as ΔM is removed, coupling it to the orbit as described above. This ΔM , however, is now removed from the system so that the change in orbital angular momentum is,

$$(\Delta J_{\text{orb}})_{\text{new}} = \Delta J_{\text{orb}} - \Omega_{\text{K}}(R_{\text{m}}) R_{\text{m}}^2 \Delta M, \quad (6)$$

where $\Omega_{\text{K}}(R_{\text{m}})$ is the Keplerian angular velocity at the magnetospheric radius. The accretor spins down according to

$$(\Delta J_{\text{a spin}})_{\text{new}} = \Delta J_{\text{a spin}} - (\Omega_{\text{K}}(R_{\text{m}}) - \Omega_{\text{a}}) R_{\text{m}}^2 \Delta M. \quad (7)$$

We limit the time step so that the second term on the right side of Eqn. 7 does not introduce numerical instabilities.

Through accretion and propeller evolution an equilibrium spin period can be achieved, which produces a ‘spin up line’ in the pulsar spin period-magnetic field distribution. Following the magnetic dipole model of Arzoumanian, Cordes, Wasserman (1999, equ. 2) we adopt the spin up line given by $B_{\text{eq}} = f_{\text{eq}} 1.025 \times 10^{12} P^{7/6}$, where the spin period, P , is expressed in seconds, the critical equilibrium magnetic field, B_{eq} , is in Gauss and f_{eq} is a parameter encapsulating the uncertainties in the relation and is of order unity. In this picture, the pulsar spins up when $B < B_{\text{eq}}$, spins down when $B > B_{\text{eq}}$, and is held at the spin equilibrium period when $B \sim B_{\text{eq}}$. To prevent the system from alternating between these two states in successive time steps, when $B \sim B_{\text{eq}}$, some fraction (typically half) of the mass is allowed to accrete during that time step with a concomitant decrease in the field (see §2.3). The pulsar is now forced to rotate at the spin equilibrium of the new pulsar magnetic field, and the pulsar evolves along the spin up line to shorter spin periods provided that equilibrium can be maintained. During the equilibrium phase, the rotation of the accretor is coupled to the orbit similar to Eqn. 6. If ablation occurs during the operation of the propeller mechanism (either spin down or the equilibrium scenario), we ignore the propeller mechanism and instead implement the ablation mechanism as described below (because the matter is ejected before arriving at the magnetosphere of the NS). In addition, the accreting NS is not allowed to spin up beyond the spin equilibrium line.

2.1.3 Ablation evolution

Ablation of the companion can occur if the rate of energy deposition into its envelope is sufficiently high. This can result from irradiation of the companion by the pulsar as a consequence of the pulsar electromagnetic radiation and/or its relativistic wind. For a donor star sufficiently close to its NS companion, matter can be lifted off its surface and lost from the system. During the ablation phase the rate of mass loss from the companion, \dot{M}_{ablated} , follows from the simple prescription of van den Heuvel & van Paradijs (1988) such that,

$$\dot{M}_{\text{ablated}} = f_e \left(\frac{2}{V_{\text{esc}}^2} \right) \left(\frac{R_{\text{d}}}{2a} \right)^2 \frac{2R_{\text{a}}^6 B_{\text{s}}^2}{3c^3} \left(\frac{2\pi}{P} \right)^4 \quad (8)$$

Here V_{esc} is the escape velocity of the companion and f_e is an efficiency factor for converting the pulsar luminosity into mass loss. As this factor is not well determined, it is treated as a parameter, which unless otherwise stated is taken to be 0.1%. We note that a value of 0.1% is a conservative choice in comparison to estimates of the ablation efficiency adopted by van den Heuvel & van Paradijs (1988), Phinney et al. (1988), and Ruderman, Shaham & Tavani (1989). When the donor is a giant star we limit the mass ablated in one time step, Δt , to be no more than the mass of the envelope – in practice this only becomes important when the majority of the envelope has already been lost. For completeness, we also require $\dot{M}_{\text{ablated}} < M_{\text{d}}/\Delta t$. The donor mass is updated accounting for both the RLOF mass loss and the ablation mass loss. For the latter, the material removed from the orbit is described as a wind from the companion. The change in orbital angular momentum is given by

$$(\Delta J_{\text{orb}})_{\text{new}} = \Delta J_{\text{orb}} - \frac{(\Delta M_{\text{ablated}})M_{\text{a}}^2}{M_{\text{tot}}^2} a^2 \Omega_{\text{orb}} \sqrt{1 - e^2}. \quad (9)$$

The specific angular momentum of the matter lost from the system due to the donor is $M_{\text{a}}/M_{\text{d}}$ times the specific angular momentum of the binary system. This loss coupled with the mass loss from the system due to ablation of the companion will tend to lead to an increase in orbital period. The corresponding change in the spin of the star is,

$$(\Delta J_{\text{d spin}})_{\text{new}} = \Delta J_{\text{d spin}} - \Delta M_{\text{ablated}} R_{\text{d}}^2 \Omega_{\text{d}}. \quad (10)$$

The ablation mechanism is allowed to occur even when the companion does not fill its Roche lobe, as long as the pulsar is sufficiently powerful.

2.2 Distinguishing between accretion, ablation and propeller

The regimes distinguishing the phases of accretion, ablation and propeller can be delineated by comparison of the light cylinder radius, magnetospheric radius, and the corotation radius. The light cylinder radius, $R_{\text{lc}} = cP/2\pi$, defines the radius at which matter coupled to the magnetic field rotates at the speed of light, c . The magnetospheric radius, is defined in §2.1.1. The co-rotation radius, $R_{\text{co}} = (GM_{\text{NS}}P^2/4\pi^2)^{1/3}$, represents the radius for which the Keplerian angular velocity in the accretion disk is equal to the NS angular velocity. For cases where the magnetosphere breaches the light cylinder ($R_{\text{m}} > R_{\text{lc}}$), the magnetospheric emission in the pulsar may be activated facilitating ablation. On the other hand, propeller action can be enabled if $R_{\text{m}} > R_{\text{co}}$.

Analogous to the magnetospheric radius, which is important in determining the evolutionary phases of the system, there exists critical mass accretion rates that determine the evolution in our study. We adopt the critical accretion rate, $\dot{M}_{\gamma\text{c}}$, derived by Takata, Cheng & Taam (2010; their equ. 10),

$$\dot{M}_{\gamma\text{c}} = 3.3 \times 10^{-12} P_{-3}^{1/2} B_8^{1/2} s_1^{1/2} R_6^{3/2} E_{0.1}^{-2} M_{1.4}^{-1} M_{\odot} \text{yr}^{-1}, \quad (11)$$

where the pulsar may halt accretion. Here, P_{-3} is the NS rotational period in units of 10^{-3} s, B_8 is the NS magnetic field in units of 10^8 G, s_1 is the ratio of curvature radius of the magnetic field line to the light cylinder radius and assumed to be unity, R_6 is the NS radius in 10^6 cm, $E_{0.1}$ is the X-ray photon energy in units of 100 eV, and $M_{1.4}$ is the NS mass in units of $1.4 M_{\odot}$.

An additional critical rate is associated with the stability of the accretion disk since we assume that the pulsar can turn on during the quiescent state of the system when it exhibits X-ray transient phenomena (see below). The latter critical accretion rate depends upon the composition of the disk and on the degree of irradiation (Lasota, Dubus & Kruk 2008). For a helium (He) star or He WD we use the He disk models, whereas H disk models are used for MS or giant star companions. For simplicity we only consider the irradiated disk models (Lasota, Dubus & Kruk 2008) and assume that the outer edge of the disk extends to 0.8 times the NS Roche radius, however, we included the non-irradiated case as an option within BSE. The pure hydrogen equation is (Lasota, Dubus & Kruk 2008; Appendix A),

$$\dot{M}_{\text{irr}} = 1.5 \times 10^{-11} R_{10}^{2.39} M_1^{-0.64} M_{\odot} \text{yr}^{-1}, \quad (12)$$

and the helium disk equation is,

$$\dot{M}_{\text{irr}} = 3.3 \times 10^{-10} R_{10}^{2.51} M_1^{-0.74} M_{\odot} \text{yr}^{-1}. \quad (13)$$

Here R_{10} is the outer disk radius in units of 10^{10} cm and M_1 is the NS mass in solar units.

Given the radii defined above, there exist four regimes of importance for the evolution of the system. **(1)** In cases for which $R_{\text{m}} < R_{\text{co}}$ and $R_{\text{m}} < R_{\text{lc}}$ accretion occurs since neither ablation nor propeller evolution develops. **(2)** If $R_{\text{m}} > R_{\text{co}}$ and $R_{\text{m}} < R_{\text{lc}}$, the pulsar can not ablate the companion, but the propeller mechanism can operate. **(3)** When $R_{\text{m}} < R_{\text{co}}$ and $R_{\text{m}} > R_{\text{lc}}$ it is possible for the pulsar to ablate its companion without the action of the propeller phase taking place. For mass accretion regimes in which the accretion disk is unstable ($\dot{M} < \dot{M}_{\text{irr}}$), we assume the pulsar is activated during the first quiescent phase. If the gamma-ray irradiation mechanism is effective

($\dot{M} < \dot{M}_{\gamma c}$) accretion is halted and ablation occurs. (4) Finally, both propeller and ablation can occur if $R_m > R_{co}$ and $R_m > R_{lc}$. To avoid unnecessary complication, we assume that during the ablation phase of the MSP companion, material is directly ejected from the system and not transferred to the disk.

2.3 Population synthesis method

The binary population synthesis is performed using BINPOP, a package developed in Kiel et al. (2008). BINPOP employs a rapid Binary Stellar Evolution (BSE) algorithm as described in Hurley, Tout & Pols (2002)¹ and Hurley, Pols & Tout (2000), with updates provided in Kiel & Hurley (2006), Kiel et al. (2008) and Kiel & Hurley (2009). An important addition to BSE, for this work, was the inclusion of pulsar physics in both isolation and binary systems (Kiel et al. 2008), allowing the user to follow pulsar magnetic braking and magnetic field decay (Ostriker & Gunn 1969), accretion induced field decay and spin up, propeller evolution, pulsar death lines and electron capture SNe.

Each system, initially comprised of two MS stars, is evolved from a random birth age, between $0 - T_{\max}$, to the assumed age of the Galaxy, $T_{\max} = 12$ Gyr. This leads to an assumed time independent star formation rate, the magnitude of which can be scaled when calculating formation rates (see § 5). The initial binary values and standard evolution assumptions used here closely follow Table 1 of Kiel, Hurley, & Bailes (2010), unless otherwise stated.

For our base model (Model A) accretion induced field decay is chosen to follow an inverse function (equ. 9 of Kiel et al. 2008) with a scaling factor of $M_{\star} = 10^{-4} M_{\odot}$ (Shibazaki et al. 1989) and a pulsar magnetic field decay timescale of 900 Myr. This form of decay is adopted as the overall shape of the theoretical pulsar distribution better reproduces the observed distribution of pulsars in the spin period-spin period derivative diagram than equ. 8 of Kiel et al. (2008). Three supernova Maxwellian kick distributions are adopted which correspond to core collapse (with a dispersion of $\sigma_{CC} = 265 \text{ km s}^{-1}$), accretion induced collapse ($\sigma_{AIC} = 90 \text{ km s}^{-1}$), and electron capture (as defined by Kiel et al. 2008; $\sigma_{ECS} = 90 \text{ km s}^{-1}$).

LMXBs have smaller orbital separations than the radii of their compact object progenitor. A solution was suggested in Paczynski (1976), where two compact cores (in this case a compact core can be a MS star) spiraled in towards each other within a common envelope. Friction from the stellar passage within the envelope is

assumed to drive off the envelope at the expense of orbital energy. One of the compact objects was the core of a giant whose envelope supplied the common envelope now shared by the two cores. The other core can be a highly evolved star (BH, NS or WD) or a MS star.

In LMXB formation the entire envelope needs to be removed and a surplus of orbital angular momentum to remain if a close binary is to exist. This simple scenario leads to an energy balance equation of CE evolution, of which the uncertainties are encapsulated into two parameters, the CE efficiency parameter, α_{CE} , and the stellar structure parameter, λ , related to the binding energy of the CE. Much uncertainty surrounds the evaluation of α_{CE} (Tutukov & Yungelson 1996; Kiel & Hurley 2006), however, typically $\alpha_{CE} = 1$ (Willems & Kolb 2002; Pfahl et al. 2003; Voss & Tauris 2003; Kiel & Hurley 2006), $\alpha_{CE}\lambda = 1$ (Belczynski et al. 2002; Nelemans & Tout 2005; Pfahl, Podsiadlowski & Rappaport 2005; Belczynski et al. 2008) or $\alpha_{CE} = 3$ (Kiel & Hurley 2006; Kiel et al. 2008; Kiel, Hurley & Bailes 2010; Hurley et al. 2010).

The treatment of the CE process itself varies and can result in different values of α_{CE} corresponding to equivalent efficiencies. For example, in BSE the binding energy to be driven off is that of the giant star prior to the CE event,

$$E_{\text{bind}} = -\frac{GM(M - M_c)}{\lambda R}, \quad (14)$$

where G is the gravitational constant, M is the donor mass, M_c is the donor core mass, R is the donor radius and λ is the donor stellar structure parameter. This binding energy is balanced by the difference between the initial orbital energy of the binary,

$$E_{\text{orb},i} = \frac{-GM_c m}{2a_i} \quad (15)$$

and the final orbital energy,

$$E_{\text{orb},f} = \frac{-GM_c m}{2a_f} \quad (16)$$

such that,

$$\frac{M(M - M_c)}{\lambda R} = \frac{\alpha_{CE} M_c m}{2} \left(\frac{1}{a_f} - \frac{1}{a_i} \right) \quad (17)$$

Here m is the compact object, a_i is the initial orbital separation at the onset of CE and a_f is the final orbital separation once the envelope has been entirely removed. An alternative formulation of the CE prescription takes the binding energy between the envelope mass and the combined mass of the two compact objects (Iben & Livio 1993; Yungelson et al. 1994),

$$E_{\text{bind}} = -\frac{G(M + m)(M - M_c)}{\lambda R}, \quad (18)$$

¹Freely accessible at <http://astronomy.swin.edu.au/~jhurley/>

or the entire donor mass is used in the initial orbital equation (Webbink 1984; de Kool 1990; Podsiadlowski et al. 2003; Belczynski et al. 2008),

$$E_{orb,i} = \frac{-GMm}{2a_i}. \quad (19)$$

In this latter prescription a value of $\alpha_{CE} = 1$ is equivalent in efficiency to a value of $\alpha_{CE} \sim 3$ in the BSE method (see Kiel & Hurley 2006; Hurley et al. 2010).

The stellar structure parameter is another source of uncertainty in the CE prescription. Although the value is known to vary with stellar type and age, many previous models have assumed a constant value, typically $\lambda = 0.5$ (Portegies Zwart & Yungelson 1998; Hurley, Tout & Pols 2002; Belczynski et al. 2002; Podsiadlowski, Rappaport & Han 2003). The variation with stellar age has also been examined in detailed stellar evolution codes (Dewi & Tauris 2001; Ivanova & Taam 2003; Podsiadlowski et al. 2003), where λ is shown to vary between 0.02 – 0.7. Population synthesis calculations that use a non constant value of λ are Voss & Tauris 2003; Podsiadlowski et al. 2003; Kiel & Hurley 2006; Kiel et al. 2008, 2010; Hurley et al. 2010). Since its inception BSE has been updated to include an algorithm that calculates a value of λ based on comparison to the detailed models of Pols et al. (1998), see Kiel & Hurley (2006) and Hurley et al. (2010).

Detailed treatment of the CE process with hydrodynamic models has been attempted (Bodenheimer & Taam 1984; Taam & Sandquist 2000; Ricker & Taam 2008; Podsiadlowski et al. 2010), but has yet to produce a cohesive physical understanding of the entire process. Podsiadlowski et al. (2010) present an intriguing scenario which shows the simplicity of the α -formalism (Nelms & Tout 2005).

The evolution of short period systems is determined by the angular momentum losses associated with magnetic braking of the companion (Schatzman 1962). When tidally coupled the spin down of the star owing to magnetic braking removes angular momentum from the orbit to maintain the spin-tidal coupling. We use Eqn. 50 of Hurley, Tout & Pols (2002), which corresponds closely (within a factor of 3) to the prescription developed by Verbunt & Zwaan (1981) as

$$\dot{J}_{mb} = -5.83 \times 10^{-16} \frac{M_{d,env}}{M_d} (R_d \Omega_{d,spin})^3 M_\odot R_\odot \text{yr}^{-2}. \quad (20)$$

Here, $M_{d,env}$ is the mass in the envelope of the donor (in this case, for low-mass MS stars the envelope mass is the entire stellar mass) and $\Omega_{d,spin}$ is the donor spin rate. We note that eqn. 20 is just one of several forms

that has been proposed over the years as other forms are given by Chaboyer, Demarque & Pinsonneault (1995), Andronov et al. (2003) and Ivanova & Taam (2003). In addition to angular momentum losses associated with magnetic braking, gravitational radiation also removes angular momentum from the orbit. Here, we make use of equations 48-49 from Hurley, Tout & Pols (2002), which under the assumption of the weak field approximation gives,

$$\dot{J}_{gr} = K_{gr} J_{orb} (1 + 7/8e^2) \quad (21)$$

and

$$\dot{e} = K_{gr} e (19/6 + 121/96e^2) \quad (22)$$

where $K_{gr} = -8.315 \times 10^{-10} \frac{M_d M_a M_{tot}}{a^4 (1-e^2)^{5/2}}$.

2.3.1 The companion

When a MS star loses sufficient mass, hydrogen burning cannot be maintained, and the stellar structure changes from a low mass, fully convective, star to a star supported by electron degeneracy pressure. The degenerate configuration is approximated by a $R \propto M^{-1/3}$ power law, and for the simplest of assumptions (zero temperature) the radius is roughly a factor of $2.5 \sim (1+X)^{5/3}$ times larger than a He WD of the same mass. However, the temporal history of the mass transfer and binary evolution up to this transition leads to departures from this simple description. It should be pointed out that within BSE the properties of the mass transferring components are calculated from fits to detailed models of stars in thermal equilibrium. In addition, the low mass MS like stars in a state of mass transfer originating from stars more massive than $1 M_\odot$ do not account for deviations of the central hydrogen content associated with nuclear evolution which lead to shorter orbital periods than obtained by using a mass-radius relation given by Eqn. 23.

For the low mass short orbital period binaries the thermal timescale of the donor is long compared to the mass loss timescale. For example the Kelvin-Helmholtz timescale for a MS star near the orbital period minimum, corresponding to a mass $M \sim 0.07 M_\odot$, is $\tau_{KH} \sim 4 \times 10^9$ yr, which increases with decreasing mass. On the other hand, the mass transfer time scale for systems near the minimum orbital period are $< 2 \times 10^9$ yr. Therefore, these stars will be out of thermal equilibrium and not fully degenerate. This departure from thermal equilibrium results in so called thermal bloating for which the radius of the star is larger than in a fully degenerate state. Although it is desirable to include the affect of thermal bloating in detail in our synthesis,

we follow the parameterization of the mass radius relation governing low mass hydrogen stars adopted in BSE (see Eqn. 24 in Hurley, Tout & Pols 2002), so that the partially degenerate MS radius is,

$$R_{\text{MS}} = 0.0128 (1 + X)^{5/3} k \left(\frac{M_d}{M_\odot} \right)^{-1/3} R_\odot. \quad (23)$$

We note that Hurley, Tout & Pols (2002), following Tout et al. (1997), implicitly assumed these stars to be out of thermal equilibrium and that $k = 2$. The form of this equation follows Tout et al. (1997), and is parameterized in a similar manner by Nelson & Rappaport (2003) and King et al. (2005) in their semi-analytical approaches. Here, k , is the bloating factor corresponding to the ratio of the radius to its fully degenerate zero temperature radius. Owing to the very simple prescription based method of modeling here, we do not capture this effect in a fully consistent way, but expect that the trends produced in the evolutions are not severely affected. The distended behavior of the companion star has been noted in previous studies in which similar systems were evolved in detail (Nelson & Rappaport 2003; Rappaport, Joss & Webbink 1982; Paczynski & Sienkiewicz 1981). In particular, Rappaport, Joss & Webbink (1982) and Nelson & Rappaport (2003) show clearly that an increase in angular momentum losses (shorter mass loss time scales) results in more distended companion stars.

In addition to mechanisms related to pulsar properties in driving the evolution of the system, dynamical mass transfer leading to a merger of the binary components can also take place. Following Ruderman & Shaham (1985) we assume the mass transfer from He, carbon-oxygen (CO) or oxygen-neon (ONe) WDs becomes dynamically unstable for some critical mass ratio, assumed to be ~ 0.006 (which for $M_{\text{NS}} \sim 1.35 M_\odot$ gives $M_c \sim 0.008 M_\odot$). This critical ratio is lower than the value assumed by Ruderman & Shaham (1985), but was chosen to match well with the observed minimum mass of ultra-compact MSP binaries (see § 3.1). This evolutionary phase has not been established in the general context, and we assume hydrogen-rich semi-degenerate binary components do not undergo this dynamical mass transfer.

3 Evolutionary tracks and comparison to detailed simulations

To determine the adequacy of the simplified prescription used for the binary evolution in the population synthesis, we compare our results to those obtained from a binary evolution code used in McDermott & Taam

(1989) and with results presented in Lin et al. (2011) in Figs. 1-4 and Fig. 5 respectively. For comparison to McDermott & Taam (1989) we examine two systems with companion masses at either end of the low mass X-ray binary companion mass range. Figs. 1 and 2 has a companion mass of $M_2 = 1.64 M_\odot$ when the long lived mass transfer phase begins, while Figs. 3 and 4 have $M_2 = 0.4 M_\odot$ when mass transfer is first initiated. The evolution is shown from the onset of the LMXB phase with $k = 2$, where the pulsar spin period and magnetic field are 20 s and 1.1×10^{12} G respectively. The detailed evolution of the donor was only followed to a mass $\sim 0.07 M_\odot$ because of the numerical issues in the equation of state. The magnetic braking orbital angular momentum loss methods are the same for both codes following Eqn. 20. It is important to note that in BSE the steady nuclear mass transfer rate is set by a simple function of the companion mass and ratio of companion radius to its Roche lobe, and for compact accretors there is an additional term dependent on the accretor's radius given by (see Hurley, Tout & Pols 2002; Eqn. 58),

$$\dot{M} = \frac{3 \times 10^{-3}}{\max(R_1, 10^{-4})} [\min(M_2, 5.0)]^2 [\ln(R_2/R_{2\text{RL}})]^3 M_\odot \text{ yr}^{-1} \quad (24)$$

Within Fig. 1 we artificially set the separation after the NS explosion such that mass transfer begins so that the MS star is approximately 500 Myrs old in both models. We see that the two models clearly diverge from the initial time step onwards. It is the mass transfer rate that drives these divergent evolution solutions of this system, and it is here that the two calculations differ greatly. To compensate for this difference we modified the mass transfer rate on nuclear timescales within BSE for NS and BH accretors by,

$$\dot{M}_{\text{new}} = \frac{2000}{3} \dot{M} \quad (25)$$

This alternate evolution is shown in Fig. 2 where we also ensure that the system remains in RLOF if the companion radius is decreasing with decreasing mass. As a consequence we allow mass transfer during the time in which magnetic braking ceases to act as an angular momentum sink. However, as can be seen in Figs. 1 and 3 the original BSE method still allowed mass transfer during this time as well. As such we allow the magnetic braking process to occur continuously during the detailed calculations shown here. A better treatment of this phase will be pursued at a later date.

The time evolution of the system in Fig. 2 is now similar when comparing the two codes. Although there is some discrepancy in the mass transfer rates over time,

we feel that BSE adequately captures the long-term evolution of the mass transfer rate. The difference in radius and, therefore, separation arises because of the mass difference at each point in time.

It is interesting to note that the pulsar does, eventually, begin to ablate its companion once it becomes a partially degenerate hydrogen-rich star. At this point the mass loss of the companion rapidly increases and the change in angular momentum begins to alternate between high and low values as the binary system attempts to adjust to this new phase of mass loss.

Fig. 3 depicts the temporal evolution of our $0.4 M_{\odot}$ companion mass system with the original mass transfer scenario of BSE. We artificially set the separation after the NS explosion such that mass transfer begins so that the MS star is approximately 630 Myrs old. In this case, the mass transfer rate does quite well in evolving NS-LMXBs, when compared with the detailed evolution code. However, there are differences in the mass transfer rate at early and late times and as such we again adjust the mass transfer rate and algorithm. We note that the first small drop in mass transfer rate of the BSE model (lower left corner of Fig. 3) is where magnetic braking terminates.

Increasing the mass transfer rate in BSE (Eqn. 25) again ensures a closer fit over time as compared to our detailed model. The slight divergence in the companion mass is driven by slight differences in mass transfer, along with the alternate mass required for the systems to begin with the same orbital separation. Better agreement would require fine tuning of BSE, however, it will not adversely affect our conclusions or rates as the time evolution of the ablation phase should not be overly affected. Instead, it simply affects the time at which ablation occurs. Because our population synthesis calculations have a flat distribution of birth ages, changes in the onset of ablation should not alter our statistics.

We have also compared the results of our binary evolution model with the recent study of Lin et al (2011). Although there is insufficient information provided to make direct comparisons as in Fig. 4, we can compare the evolution in terms of the orbital period versus companion mass. In Fig. 5, we take our initial system characterized by an $11.83 M_{\odot}$ primary and a $1.5 M_{\odot}$ secondary in a 740 day orbit. Evolution through a common envelope and supernova explosion leads to the formation of a system in which a $\sim 1.33 M_{\odot}$ NS and $1.5 M_{\odot}$ MS enters into a RLOF phase at a time of 500 Myr. The pulsar is born with spin period of 0.3 s and magnetic field of 2.7×10^{12} G and, at the time of mass transfer, the pulsar spin period and magnetic field are characterized by 21 s and 1.6×10^{12} G respectively. It takes only ~ 1 Myr for the pulsar to come into spin equilibrium.

In comparison to the Lin et al. (2011) model it can be seen in both panels of Fig. 5 that the evolution is very similar during the phase corresponding to the decrease of orbital period with decreasing companion mass. The major difference is seen in the phase corresponding to the increase in the orbital period with decreasing mass, with large values of k departing from the detailed calculations of Lin et al. (2011), consistent with earlier work by King et al. (2005), but also places the models closer to where many black widow pulsars are observed.

Taking into account the effects of propeller and ablation leads to lower masses and correspondingly longer orbital periods as shown in the right panel of Fig. 5. However, the orbital expansion is governed by the mass-radius relationship, and therefore the value of k , rather than the angular momentum losses from propeller evolution and ablation of the companion. It is interesting to note that the case for $k = 1$ in the lower right panel leads to an evolution which lies in the vicinity of the Lin et al (2011) curve but extends the companion masses evolution to lower masses and longer orbital periods.

3.1 Example evolutionary tracks of black widow phase

Prior to our analysis of the population synthesis characteristics of black widow systems, we first determine the companion mass-orbital period parameter space where the systems are expected to form, building on the earlier work of King et al. (2005). Here, we take the equations defined above that describe the transition to the ablation phase and with the simple assumptions for the mass-radius relation and mass transfer rate, calculate the critical transition points.

We assume the companion fills its Roche lobe with its radius determined from the companion mass-radius relationship of

$$R_{\text{MS}} = 0.0128 (1 + X)^{5/3} k \left(\frac{M_{\text{d}}}{M_{\odot}} \right)^{-1/3} R_{\odot}. \quad (26)$$

This assumption leads to an estimate of the mass transfer rate, assuming the change in angular momentum is driven by gravitational radiation, such that $\dot{M}_{\text{gr2}}/M_2 = \dot{J}/[J(2/3 - M_2/M_{\text{NS}})]$. This rate is then compared to the critical disk stability limit (Eqn. 12) of Lasota et al. (2008) and to the gamma-radiation equation (Eqn. 11) of Takata, Cheng & Taam (2010). The transition region is determined by \dot{M}_{gr2} lying below the values of both the critical limits. We assume a NS mass of $1.4 M_{\odot}$, eccentricity of zero, pulsar spin period of 5 ms, and pulsar magnetic field of 1×10^8 G. This standard setup is shown with the three lines for various companion masses and bloating factors. In addition, we also vary the NS mass, pulsar spin period and magnetic field.

Upon examining the trends exhibited in Fig. 6, it is evident that the onset of the ablation phase is most sensitive to the degree of thermal bloating of the companion. Lower values of the bloating result in shorter orbital periods and lower companion masses at the transition. A higher magnetic field strength leads to an increase of the critical mass transfer rate that determines when a pulsar may begin to halt accretion (Eqn. 11). It is this equation that, on average, determines when ablation will occur because it results in a lower critical mass transfer rate than that given by the disk stability limit (if one assumes 'typical' parameter values). Similarly, decreasing the magnetic field and spin period increases the orbital period at which the change in system state occurs. The transition region depends little on the NS mass.

Uniting together into one example each of the effects discussed above (and assuming a magnetic field of $5 \times 10^7 \text{G}$) increases the orbital period of where the transition region occurs and places it between the grey squares and circles. The observed sources are listed in Table 1. As seen from Eqns. 11 and 12 the parameters that lead to the largest variation in transition region are associated with the NS radius and accretion disk radius.

To examine the sensitivity of the evolutionary pathways for particular assumptions of our population synthesis modeling we vary parameters of our model and provide details for the variation of R_d , a , \dot{M} and \dot{J} with respect to time in Figs. 7 and 8. As an example, we use the system depicted in Fig. 4 (see caption for details). The NS within this simulation is born with $P_s = 0.3 \text{ s}$ and $B_s = 2.7 \times 10^{12} \text{ G}$ and formed soon after the system emerged from the common envelope phase with an orbital period of 0.2 day. At the start of mass transfer the NS has $P_s = 24 \text{ s}$ and $B_s = 1.3 \times 10^{12} \text{ G}$ and at the simulations end it has $P_s = 0.0007 \text{ s}$ and $B_s = 9.8 \times 10^7 \text{ G}$. In this case, the system evolves to the semi-degenerate hydrogen-rich track and is analogous to a cataclysmic variable system, but with a NS compact object. The system evolves to the black widow phase, and the pulsar fully ablates its companion. The system does not evolve by regularly passing through the ablation phase, but instead undergoes alternating phases of equilibrium mass transfer and ablation. We also point out that qualitatively, the mass accretion rate onto the NS as shown in Fig 7 is similar in shape and magnitude to those calculated by Rappaport, Joss & Webbink (1982), whose binary mass transfer was driven by gravitational radiation only.

Upon further examination of Fig. 7 a number of features are present in the panel illustrating the mass accretion rate as a function of time, which are associated

with similar changes in the variation of angular momentum. The total change in angular momentum with time (black points in Fig 7) closely follows the orbital decay owing to gravitational radiation (red stars), except for an unexpected peak as compared to the mass transfer results found by Rappaport, Joss & Webbink (1982). The sudden increase in the mass accretion rate reflects the slow response of the orbit to the change in stellar structure of the companion becoming partially degenerate and leading to the change in sign of the radius mass derivative. Because $\dot{M} \propto (\log R_d/R_{\text{RL d}})^3$, where $R_{\text{RL d}}$ is the donor's Roche lobe radius, the mass transfer rate increases. This result follows from the fact that the Roche lobe radius is not forced to be the stellar radius exactly, when the radius increases. Therefore, over a small number of time steps the orbit continues to decay while the companion radius increases. These features occur over a relatively short time scale and are due to our assumptions in the code and the time explicit method of time integration. It is unlikely that their influence is significant as the perturbations are small. For the most part the separation of the two stars follows the change in companion radius.

We have also examined the sensitivity of our results to the magnetic field decay rates. Specifically, lowering the value of M_\star increases the rate at which the magnetic field decays with accreted mass. The effect of setting $M_\star = 10^{-6}$ is shown in Fig. 8 and results in an evolution where the pulsar never has the power to ablate its companion. The mass transfer rate evolution is similar to that described in Fig. 7.

To examine the dependence of the evolution of the systems to the equilibrium spin relation, we increased f_{eq} from 0.5 to 1. That is, the NS is on the equilibrium line at higher magnetic fields, or for the same field strength the equilibrium spin is at a faster rate. This causes the ablation process to occur at a later time (by $\sim 400 \text{ Myr}$). Interestingly, the time spent in ablation is shorter as more angular momentum losses lead to higher mass transfer rates, which in turn depletes the companion faster. Ablation lasts for only a few tens of millions of years.

Adopting a lower efficiency of conversion of pulsar luminosity to mass loss by decreasing the value of f_e from 0.1% to 0.01% decreases the fraction of mass ablated from the companion by up to an order of magnitude at early times, and reduces the rate of orbital angular momentum loss. As a consequence the system lives longer by $\sim 1 \text{ Gyr}$.

If we decrease k , the orbital evolution of the companion, during ablation, is affected. In this case, ablation of the companion occurs prior to the orbital period minimum. Here, the orbital angular momentum

Table 1 Characteristics of the observed black widow pulsar systems ordered in ascending orbital period.

Name	M_2 [M_\odot]	porb [day]	P [s]	\dot{P} [s/s]	Ref.
J2051-0827	0.03	0.099	0.00451	1.27e-20	Stappers et al. (1996)
J1544+4937	0.018	0.117	0.00216	—	Kerr et al. (2012), Roberts (2012)
J2047+10F	0.035	0.125	0.00429	—	Ray et al. (2012), Roberts (2012)
J0023+09F	0.018	0.138	0.00305	—	Hessels et al. (2011), Roberts (2011)
J2241-5236	0.014	0.146	0.00219	6.64e-21	Keith et al. (2011)
J1810+17F	0.050	0.15	0.0023	—	Hessels et al. 2011, (Roberts 2011)
J2256-1024F	0.039	0.213	0.00229	—	Boyles et al. (2011), Gentile (2012)
J1124-3653	0.027	0.225	0.00241	—	Hessels et al. (2011), Roberts (2012)
J1301+0833F	0.024	0.271	0.00184	—	Ray et al. (2012), Roberts (2012)
J1446-4701	0.02	0.277	0.00219	—	Keith et al. (2012)
J0610-2100	0.02	0.286	0.00386	1.24e-20	Burgay et al. (2006)
J1731-1847	0.043	0.311	0.00234	2.49e-20	Bate et al. (2011)
J1959+2048	0.02	0.382	0.00161	1.69d-20	Fruchter et al. (1988)
J2214+3000	0.03	0.417	0.00312	1.401e-20	Ransom et al. (2011)
J2234+0944F	0.015	0.417	0.00363	—	Roberts (2012)
J1745+1017F	0.016	0.729	0.00265	—	Barr et al. (2013), Roberts (2011)

losses drive this system to the period minimum within 100 Myr from the onset of ablation. This evolution was not explored in our previous examination of the transition phase into ablation and occurs at an orbital period of 0.05 day and a companion mass of $0.098 M_\odot$. As an additional result associated with a decreasing value of k , we note that the mass ablation rate increases and the pulsar spends a greater time ablating its companion compared to the values in Fig 7 because the two stars are now closer together. In this case, the companion mass decreases more rapidly, quickly leading to the formation of an isolated MSP.

4 Example evolutionary outcomes over a range of initial systems

The results of our population synthesis simulations, and in particular two models which comprise our ‘standard’ assumptions, are presented below. These two models differ in one respect, viz., model A (B) does not (does) include propeller evolution and/or ablation of the companion. For convenience, we provide the typical values for some of the more important parameters here. Specifically, we evolve $N = 3 \times 10^8$ binary systems. For each CE we assume $\alpha = 3$, while we include a variable binding energy constant, λ , as discussed above. NSs can be born via either core collapse or electron capture SNe (which includes accretion induced collapse), and we assume the resultant SN asymmetric kicks are drawn from a Maxwellian distribution (see §2.3). When a pulsar evolves to longer spin periods we allow the field to decay exponentially on a timescale of $\tau_B = 900$ Myr, while in isolation and decay with mass accreted during the mass accretion phase with $M_\star = 1 \times 10^{-4} M_\odot$.

These models are based on the modified mass transfer rate provided in Eqn. 25 for NSs accreting from MS stars. We force this mass transfer to continue until a physical process such as the propeller phase leads to its termination. Each system is born at a random time in the Galaxy’s history, resulting in a flat distribution of birth ages between 0 – 12 Gyr.

Before examining the results from our population synthesis simulations we first briefly discuss the initial properties of those systems that become black widow MSPs in Fig. 9. A number of interesting features of the initial systems required to form a black widow system are depicted. The most important and interesting feature gleaned from this figure is that small mass ratio systems are more prominent than higher ones in forming black widow systems. The majority of progenitor NS masses reside between $8.5 - 10 M_\odot$ with islands in the parameter space at $15 M_\odot$ and $22 M_\odot$. Most initial companions are less massive than $0.5 M_\odot$. This is primarily a selection effect, as it is easier for lower mass stars to reach binary properties (orbital periods and pulsar characteristics) that can initiate ablation of the companion in shorter periods of time than more massive companion stars. This results from the fact that lower mass companions must spiral in deeper in the envelope during the CE phase for successful ejection.

We find that there is no significant change to this finding when other parameters are modified. The initial orbital periods of black widow systems mostly lie in a band of periods between ~ 650 days and ~ 2500 days, which does not change significantly with changes to $\alpha = 1$ and $\lambda = 0.5$. The only noticeable effect is a greater range of initial orbital period. A modification of the initial mass ratio distribution to a flat distribution leads to a reduction in the statistics. However,

the distribution of initial P_{orb} and q still reflects that of Model B—with the highest density region lying at $q \sim 0.04$, although there is a greater number of systems (relatively) residing at q between 0.1 – 0.2. The initial orbital period distribution in this case is very similar to Model B.

To demonstrate the influence of mass loss from the system due to ejection from the accretion disk by propeller action and the ablation of the companion by the pulsar on the MSP evolution, we consider the numerical results from the population synthesis of the two models. A binary MSP population corresponding to the standard mass transfer assumptions is adopted for model A, whereas model B includes propeller and ablation evolution. We note that (i) model A is comparable to a typical model from the recent study of Hurley et al. (2010), but with our updated mass transfer rate and algorithm and (ii) there is a large orbital period dependence upon k .

To illustrate the importance of propeller and ablation evolution in the formation of rotation and accretion powered MSPs (pulsars with $P < 0.03$ s) we provide a comparison of models A and B in the orbital period/companion mass plane (see Fig. 10; where only 1/100 of the model statistics is shown for clarity). Both models clearly exhibit the existence of two branches where the orbital period increases with decreasing companion mass. The upper branch describes the MS-MSP population whereas the lower branch depicts WD-MSPs (UCXBs). In model A all systems are mass transferring (i.e., LMXB's) and the separation of the two branches in orbital period results from differences in the donor radii (see §1). In this model (where $k = 2$), hydrogen-rich stars reach a mass of $\sim 0.025 M_{\odot}$ within a Hubble time, which sets a lower mass limit to donors evolving from the MS branch. We note that fully degenerate hydrogen-rich companions (where $k = 1$) may reach masses $< 0.01 M_{\odot}$ within a Hubble time due to higher angular momentum losses associated with gravitational radiation at shorter orbital periods. On the other hand, the results of model B reveal the existence of systems where the companion has detached from its Roche lobe and mass accretion has abruptly ceased. In this model, radio pulsars form in systems extending to lower companion masses on the low mass semi-degenerate branch of the MS with the evolution driven by ablation of the donor stars while the systems are evolving on the equilibrium spin line. We point out that the operation of the propeller mechanism is essential for facilitating the onset of pulsar activity and the subsequent ablation of the companion.

Many of the systems with partially degenerate hydrogen-rich companions in model B alternate be-

tween various evolutionary phases, however, the ‘accretion on the equilibrium’ phases (yellow triangles) dominates the majority of times for most systems with the pulsar spending half of this phase ‘on’ and in propeller mode so as to maintain equilibrium spin (see §2.1.2). The influence of modifying the companion thermal bloating parameter, k , is illustrated in Fig. 10, where we show the result for $k = 1, 2$ and 3 on the binary population. As expected a smaller (larger) value of k results in tighter (larger) orbits and lower (longer) minimum orbital periods. We remark that empirically, and prior to any complicating effects associated with propeller or ablation, $k = 2$ apparently matches the two observed X-ray binaries on this evolutionary branch (right most squares in Fig. 10). The primary affect of k , in this context, is to cause enhanced expansion of the orbit with increasing values of k . Examination of Fig. 10 and integration of Eqn. 9 reveal that even with the operation of the propeller and ablation mechanism the orbital evolution is dominated by our choice of k . Therefore, we emphasize that the choice of k primarily determines the black widow orbital evolution (see also King et al. 2005). That is, the thermal bloating of the companion governs the orbital evolution, while propeller and ablation evolution facilitates the transformation of an LMXB into a MSP binary.

As noted above it is evident that the longer orbital periods obtained in the present work, compared to the models of Lin et al. (2011), are a direct consequence of the value of k adopted. This may suggest that mechanisms not considered for driving the donor further out of thermal equilibrium are required (see below). Provided that such a mechanism exists, we further explore the consequences of our model results on the properties of this population. In particular, we find that there are three distinct regions of interest in $P\dot{P}$ phase space in model B as shown in Fig. 11. The lower branch represents systems characterized by an asymptotic magnetic field assumed as $B_{\text{bot}} = 5 \times 10^7$ G (see Kiel et al. 2008). The accumulation of systems in the vicinity of this branch reflects the fact that the magnetic field decays slowly with the accretion of mass as the field approaches this asymptotic value. The near vertical line at $P = 0.0016$ s consists of accreting WD-MSP systems and reflects the angular momentum accretion timescale increasing with shorter spin periods. The third branch, corresponding to large spin period derivatives, represents the equilibrium spin up line. Accumulation of systems on this line can occur at slower spin periods if we decrease the mass transfer rate, as this evolution is driven by timescales, although spin up and field decay occur slower as less mass is accreted. Here, the binary evolution is dominated by accretion and the action of

the propeller mechanism. In this model we limit the minimum pulsar spin period to its mass shedding limit, a value $P_s \sim 0.00025$ s. The MS-MSP systems that do not lie on the equilibrium line are characterized by a shorter angular momentum accretion timescale, reflecting the differing progenitor systems, as compared to their WD-MSP counterparts. Hence, they ‘flow’ from right to left through the near vertical WD-MSP line towards the asymptotic field limit.

The numerical results of model B also reveal that the ablating systems reside near the observed black widow systems in the spin frequency/orbital period plane (see Fig. 12). Although the entire observed range is covered in both orbital period and spin frequency, the systems in the high density region of our model are spinning too slowly. The LMXB’s without ablation lie at shorter orbital periods. The fact that accreting systems with MS companions on the spin equilibrium line typically have shorter orbital periods than those undergoing ablation highlights the importance of \dot{M} and the pulsar properties in MSP formation while on the degenerate (or partially degenerate) tracks.

5 Black widow population synthesis results: formation rates and predicted numbers

The formation rates of the systems of interest are calculated following the methodology of Belczynski et al. (2002) and employed by Voss & Tauris (2003), Pfahl et al. (2005) and Kiel, Hurley & Bailes (2010). The rate is the ratio of the number of systems produced (M_N) over the number of Type II SN produced within the model (M_{SNII}). This ratio is normalised to the observed Galactic Type II SN rate as estimated empirically, $R_{\text{SNII}} = 0.01 \text{ yr}^{-1}$ (Cappellaro, Evans & Turatto 1999). Taking into account the fraction of binaries, f_B , the rate equation is,

$$R = f_B R_{\text{SNII}} \frac{M_N}{M_{\text{SNII}}}. \quad (27)$$

The estimated values of our model formation rates are shown in Table 2. It can be seen that all the black widow birth rates reside within a narrow range between $4.8 \times 10^{-8} - 3.3 \times 10^{-7} \text{ yr}^{-1}$. Decreasing the lifetime of pulsars by setting $\tau_B = 100 \text{ Myr}$ (Model C) produces the greatest effect on the birth rate of black widow systems by causing many of the pulsars’ magnetic fields to decay to the assumed bottom field value of $5 \times 10^7 \text{ G}$. That is, the particle acceleration mechanism is prevented and the evolution is described by continuous accretion. Decreasing the common envelope efficiency for a fixed stellar structure parameter

(Model D) halves the birth rate and number of black widow systems estimated within the Galaxy, as compared to Model B. Setting $k = 1$ (Model E) reduces the birth rate slightly, but more significantly decreases the average black widow age and reducing the estimated number of black widows.

Assuming the companion mass function is flat in mass ratio (Model F) increases the average mass ratio value, causing a decrease in the number of LMXBs and therefore black widow systems, consistent with the results of Willems & Kolb (2002) and Hurley et al. (2010). The average age of the black widow systems also decreased by a factor of 2 to $\sim 250 \text{ Myr}$, as compared to Model B. Using the older mass transfer rate form (Model G), which is a lower rate than used in Model B, leads to an increase in the birth rate of black widow systems with respect to Model B and their LMXB counterparts. This lower rate of mass transfer falls below the critical values that define black widow formation (Equations 11–13) more readily than those LMXBs of Model B. Model H, where $M_* = 1 \times 10^{-6}$, highlights the importance of the magnetic field strength in forming black widow systems. In Section 3 we showed that assuming such a low value of M_* arrested ablation of the companion by the pulsar and this is the case here. The birth rates of black widow systems in Model H decreased substantially compared to Model B and we find that only 5 black widow systems would be observable.

Because we examine only a subset of the binary MSP population the black widow rates are much less than previous binary MSP estimations which, instead, considered the total binary MSP population and ranged from $1 \times 10^{-6} - 4 \times 10^{-4} \text{ yr}^{-1}$ (Lorimer 1995; Cordes & Chernoff 1997; Lorimer 2008; Hurley et al. 2010).

The original binary MSP estimates led to the binary MSP birth rate problem in which the model estimates of the MSP birth rates were higher by up to 2 orders of magnitude than estimated for LMXB birth rates (as initially discussed using semi-empirical arguments by Kulkarni & Narayan 1988). These estimates placed the LMXB binary birth rate at $\sim 10^{-7} \text{ yr}^{-1}$ assuming an observable X-ray lifetime of $\sim 10^9 \text{ yr}$ (Pfahl, Rappaport & Podsiadlowski 2003; Hurley et al. 2010).

We show that the LMXB rates given in Table 2 are more consistent with the black widow birth rates. However, the inconsistency may still exist from the wider binary MSP population for which the formation scenarios that exist vary greatly and do not necessarily require a long lived LMXB phase to form. The fundamental reason for our better consistency between birth rates is simply that we are examining two populations where one forms directly (and solely) from the other.

However, the necessity for thermal bloating in the models required for matching the observed orbital period-companion mass distribution may provide another possible reason of the overestimate of the LMXB age of 10^9 yr (along with irradiation induced mass transfer cycles suggested by Pfahl, Rappaport & Podsiadlowski 2003). We suggest that the thermal bloating on the degenerate track is a result of evolution on time scales shorter than the thermal timescale of the donor and, hence, the ages of LMXBs will be overestimated if the evolution is assumed to proceed on the thermal timescale. If the time spent in the X-ray binary phase is less than 10^9 yr, and account is taken of the duty cycle of accretion activity, the birth rate problem can be somewhat alleviated.

6 Discussion

The results of our simulations (Model B) reveal that systems can be produced with orbital periods as long as 0.4 days and with companion masses as low as $0.005 M_{\odot}$, with the orbital period depending upon the thermal bloating factor. In contrast, without thermal bloating ($k = 1$) systems form with masses as low as $\sim 0.002 M_{\odot}$ and orbital periods $\gtrsim 0.15$ days before they are destroyed. In general, our model systems become rotation powered MSPs in a similar region of the orbital period/companion mass plane where the observed LMXBs apparently turn into radio MSPs. We find a dependence on the bloating factor for the orbital period at which the transition from the LMXB phase to MSP occurs, however, this dependence is mitigated somewhat if the system undergoes the transition prior to the companion reaching a sufficiently low mass to become semi-degenerate (especially for $k = 1$). This transition typically occurs at $P_{\text{orb}} \sim 0.1$ days. Without the effects of propeller action and ablation (see model A), the mass accretion varies continuously and the evolution to the rotation powered MSP phase is inhibited. This latter model is similar to the models of Hurley et al. (2010), which well describes the observed LMXB population along the UCXB WD branch (e.g., SWIFT J1756.9-2508) with lower mass companions and the MS branch (e.g., SAX J1808.4-3658) for higher mass companions. However, the MS branch in models without propeller action and ablation does not extend to sufficiently low masses to describe many observed systems (e.g., J2241-5236, which has $P_{\text{orb}} = 0.146$ days and a minimum companion mass of $0.012 M_{\odot}$; Keith et al. 2011), assuming that thermal bloating is important.

The systems that are regularly accreting while on the equilibrium line will be more difficult to detect as

rotation powered MSPs, either because accretion precludes the activation of particle acceleration mechanism in the pulsar magnetosphere or because the pulsed emission is heavily obscured by the ejected material. This evolutionary phase is particularly dominant at very low companion mass, $M_d < 0.016 M_{\odot}$, and is, perhaps, the reason for the observed lack of systems in this region of parameter space (although lower masses lead to lower ablated material surrounding the system). In addition, the possible occurrence of intermittent accretion during the propeller and spin equilibrium phase, as shown in numerical models of Romanova et al. (2009), may further hinder radio MSP detection.

The observations and numerical results reveal that the ablating companions are only present on the low mass semi-degenerate MS branch and absent on the UCXB branch. The lack of black widow pulsars on the latter branch (with shorter orbital periods) may reflect the higher mass transfer rates driven by the greater losses of orbital angular momentum associated with gravitational radiation characteristic of systems on this branch. This property can limit the degree of instability in the accretion disk, thereby, restricting the parameter range for the effectiveness of ablation. It is interesting to note that the WD-MSP branch approaches an orbital period of ~ 0.1 day which is where we find a transition from the X-ray binary to the MSP binary phase. This suggests that systems like HETE J1900.1-2455 with $P_{\text{orb}} \sim 0.058$ days and $M_c \sim 0.018 M_{\odot}$ (Kaaret et al. 2006) may eventually become MSP binaries. We note that HETE J1900.1 may in fact contain a hybrid (He-rich) WD companion which would result in a companion lying between the MS-WD branches, which can be seen in Fig 10 where HETE J1900.1 lies just below the $k = 1$ model. Such an evolution could have involved companions with initial masses greater than about $1 M_{\odot}$ in which nuclear evolution has occurred (e.g., Nelson & Rappaport 2003). At present BSE does not model or evolve such hybrid stars.

It has been argued by Ho, Maccarone & Anderson (2011) that the location of MSP's in the spin frequency/orbital period plane could be understood in terms of the comparisons of orbital period changes, spin up and spin down timescales. Specifically, their location depends on where spin up/down and orbital period increase/decrease dominate the evolution of the orbit and MSP spin. In contrast to the description adopted here they emphasize the importance of gravitational wave spin down of accreting NSs. However, we find an evolution including propeller and ablation physics during the LMXB phase naturally leads to the absence of accreting MSPs at long orbital periods (> 0.1 day) and low spin frequencies (< 600 Hz) without the necessity

Table 2 Characteristics of the main set of models used in this work and the resultant formation rates and estimated number of black widows in the Galaxy now. Here $R_{\text{SNII}} = 0.01 \text{ yr}^{-1}$ (Cappellaro, Evans & Turatto 1999) and $f_{\text{B}} = 0.5$. We vary models to have different pulsar field decay timescales, τ_{B} , companion thermal bloating, k , field decay parameter, M_{\star} , mass transfer rate, mass ratio distribution and common envelope α_{CE} and λ . We include model A for completeness, however, without propeller effects or ablation of the companion, it does not produce black widow systems.

Model	τ_{B} [Myr]	k	M_{\star}	MT method	MRD	$\alpha_{\text{CE}}, \lambda$	Birth rates [yr^{-1}] LMXB::MSP	Number
A	900	2	$1e-4$	Eq. 25	KTG93	3, variable	$2.2e-5 :: N/A$	N/A
B	900	2	$1e-4$	Eq. 25	KTG93	3, variable	$1.4e-5 :: 2.2e-7$	110
C	100	2	$1e-4$	Eq. 25	KTG93	3, variable	$1.8e-5 :: 5.0e-8$	13
D	900	2	$1e-4$	Eq. 25	KTG93	1, 0.5	$6.3e-6 :: 1.0e-7$	50
E	900	1	$1e-4$	Eq. 25	KTG93	3, variable	$1.4e-5 :: 1.0e-7$	25
F	900	2	$1e-4$	Eq. 25	flat in q	3, variable	$6.2e-6 :: 6.0e-8$	13
G	900	2	$1e-4$	Eq. 24	KTG93	3, variable	$1.2e-5 :: 3.3e-7$	179
H	900	2	$1e-6$	Eq. 25	KTG93	3, variable	$2.0e-5 :: 4.8e-8$	5

for the inclusion of gravitational wave emission from a rapidly rotating NS.

7 Conclusion

A model of the formation and evolution of radio MSPs has been carried out using a binary population synthesis method (the BSE code) incorporating the effects of mass ejection from the system associated with propeller action and ablation. The accuracy of BSE to evolve LMXBs with NSs as the compact object was assessed by comparison to detailed codes of McDermott & Taam (1989) and Lin et al. (2011). As a first step in quantifying the consequences of including new input physics related to the propeller phase and ablation of the NS companion on the binary evolution, the population synthesis method was adopted to explore a large parameter range and number of systems.

It has been shown that by including both propeller and ablation physics into our models of binary and stellar evolution the companion to the neutron star in the binary system can detach from its Roche lobe transforming a LMXB to a rotation powered MSP binary. In particular, it is found that the operation of the propeller action is as crucial in this transition as the ablation mechanism. Our work also highlights the importance of thermal bloating of the companion star beyond that found in previous detailed stellar models as it relates to the orbital periods of black widow pulsar systems (see also King et al 2005).

Although the evolutionary model is promising, our model MSPs are characterized by magnetic fields that are high ($\sim 8 \times 10^8 \text{ G}$) as compared to the observed systems ($\sim 2 \times 10^8 \text{ G}$). Since this is determined by our simple spin equilibrium line, modifications to bring the model results into closer agreement with observations will be necessary. This may also be related to the

fact that the majority of our black widow systems are spinning slower than observations suggest.

Finally, the comparison of our model results with observations suggest that the degree of thermal bloating as parameterized by the factor k is ~ 2 . The magnitude of this effect may suggest that additional processes driving the mass transfer in these systems may be operating during the LMXB phase. Examples of such processes include the influence of X-ray irradiation induced stellar winds as proposed by Podsiadlowski (1991) and Iben et al. (1997) or tidal heating as hypothesized by Rasio et al. (2000). Including such effects, where it is likely that the degree of thermal bloating varies, and following the binary evolution during the LMXB phase to the binary radio millisecond pulsar phase for incorporation into detailed stellar structure and evolution models is highly desirable.

We thank the referee for his/her comments which have improved the clarity and presentation of this paper. This work was supported in part by the Theoretical Institute for Advanced Research in Astrophysics (TIARA) operated under the Academia Sinica Institute of Astronomy & Astrophysics in Taipei, Taiwan and by NASA ATP Grants NNX09AO36G and NNX08AG66G and an NSF AST-0703950 to Northwestern University. We also thank Swinburne University of Technology for use of ‘the Green machine’, the supercomputer on which the simulations were completed. PDK thanks the Academia Sinica Institute of Astronomy & Astrophysics for their hospitality during his visit.

References

- Andronov, N., Pinsonneault, M., & Sills, A. 2003, *Astrophys. J.*, **582**, 358
 Archibald, A. M., et al. 2009, *Science*, **324**, 1411
 Arzoumanian, Z., Cordes, J. M., & Wasserman, I. 1999, *Astrophys. J.*, **520**, 696
 Barr, E. D., et al., 2013, *Mon. Not. R. Astron.*

- Soc., 429, 1633
- Bates, S. D., et al. 2011, MNRAS, 416, 2455
- Belczynski K., Kalogera V., Bulik T., 2002, *Astrophys. J.*, 572, 407
- Belczynski K., Kalogera V., Rasio F. A., Taam R. E., Zezas A., Bulik T., Maccarone T. J., Ivanova N., (2008), *ApJS*, 174, 223
- Bodenheimer, P., & Taam, R. E. 1984, *ApJ*, 280, 771
- Bond, H. E., White, R. L., Becker, R. H., & OBrien, M. S. 2002, *PASP*, 114, 1359
- Boyles, J., et al. 2011, *AIPS*, 1357, 32
- Burgay, M., et al., 2006, MNRAS, 368, 283
- Cappellaro, E., Evans, R., Turatto, M., 1999, *A&A*, 351, 459
- Chaboyer, B., Demarque, P., & Pinsonneault, M. H. 1995, *Astrophys. J.*, 441, 865
- Cordes, J. M., Chernoff, D. F., 1997, *Astrophys. J.*, 482, 971
- de Kool M., 1990, *Astrophys. J.*, 358, 189
- Dewi J. D. M., Tauris T. M., 2001, in Podsiadlowski P., Rappaport S., King A. R., D'Antona F., Burderi L., eds, ASP Conf. Ser. Vol. 229, *Evolution of Binary and Multiple Star Systems*. Astron. Soc. Pac., San Francisco, p. 255
- Frank, J., King, A., & Raine, D.J. 2002, *Accretion Power in Astrophysics* (Cambridge: Cambridge Univ. Press) Fruchter, A. S., Stinebring, D. R. & Taylor, J. H., 1988, *Nature*, 333, 237
- Gentile, P., et al., 2012, arXiv:1210.7342G
- Hessels, J. W. T., et al. 2011, to appear in AIP Conference Proceedings of Pulsar Conference 2010 "Radio Pulsars: a key to unlock the secrets of the Universe", Sardinia, October 2010, ed. Burgay, M., D'Amico, N., Esposito, P., Pellizzoni, A., Possenti, A.
- Ho, W. C. G., Maccarone, T. J., & Nils, A. 2011, *Astrophys. J.*, 730, 36
- Hurley, J. R., Pols, O. R., & Tout, C. A. 2000, *Mon. Not. R. Astron. Soc.*, 315, 543
- Hurley, J. R., Tout, C. A., & Pols, O. R. 2002, *Mon. Not. R. Astron. Soc.*, 329, 897
- Hurley, J. R., Tout, C. A., Wickramasinghe, D. T., Ferrario, L., Kiel, P. D. 2010, *Mon. Not. R. Astron. Soc.*, 406, 656
- Iben I. Jr., Livio M., 1993, *PASP*, 105, 1373
- Iben, Jr. I., Tutukov, A. V., & Fedorova, A. V. 1997, *Astrophys. J.*, 486, 955
- Illarionov, A. F., & Sunyaev, R. A. 1975, *A&A*, 39, 185
- Ivanova, N, & Taam, R. E. 2003, *Astrophys. J.*, 599, 516
- Kaaret, P., Morgen, E. H., Vanderspek, R., & Tomsick, J. A. 2006, *Astrophys. J.*, 638, 963
- Keith, M. J., et al. 2011, *Mon. Not. R. Astron. Soc.*, 414, 1292
- Keith, M. J., Johnston, S., Bailes, M., et al. 2012, MNRAS, 419, 1752
- Kerr, M., et al. 2012, *Astrophys. J.*, 748, 2
- Kiel, P. D., & Hurley, J. R. 2006, *Mon. Not. R. Astron. Soc.*, 369, 1152
- Kiel, P. D., Hurley, J. R., Bailes, M., & Murray, J. R. 2008, *Mon. Not. R. Astron. Soc.*, 388, 393
- Kiel, P. D., Hurley, J. R., & Bailes, M. 2010, *Mon. Not. R. Astron. Soc.*, 406, 656
- King, A. R., Beer, M. E., Rolfe, D. J., Schenker, K., & Skipp, J. M. 2005, *Mon. Not. R. Astron. Soc.*, 385, 1501
- Kulkarni S.R., Narayan R., 1988, *Astrophys. J.*, 335, 755
- Lasota, J.-P., Dubus, G., & Kruk, K. 2008, *A&A*, 486, 523
- Lin, J., Rappaport, S., Podsiadlowski, P., Nelson, L., Paxton, B., Todorov, P., 2011, *Astrophys. J.*, 732, 70
- Lorimer, D. C., 1995, *Mon. Not. R. Astron. Soc.*, 274, 300
- Lorimer, D. L., 2008, *LRR*, 11, 8
- Manchester, R. N., Hobbs, G. B., Teoh, A., Hobbs, M. 2005, *Astrophys. J.*, 129, 1993
- McDermott, P. N., & Taam, R. E. 1989, *Astrophys. J.*, 342, 1019
- Nelemans G., & Tout C. A., 2005, *Mon. Not. R. Astron. Soc.*, 356, 753
- Nelson, L. A., & Rappaport, S. 2003, *Astrophys. J.*, 598, 431
- Ostriker, J. P. & Gunn, J. E., 1969, *Astrophys. J.*, 157, 1395
- Paczynski, B., 1976, in Eggleton, P., Milton, S., Whelan, J., eds, *Proc. IAU Symp. 73, Structure and Evolution of Close Binary Systems*. Reidel, Dordrecht, p. 75
- Paczynski, B., & Sienkiewicz, R., 1981, *Astrophys. J.*, 248, L27
- Pfahl E., Rappaport S., Podsiadlowski P., 2003, *Astrophys. J.*, 597, 1036
- Pfahl E., Podsiadlowski P., Rappaport S., 2005, *Astrophys. J.*, 628, 343
- Phinney, E. S., Evans, C. R., Blandford, R. D., & Kulkarni, S. R. 1988, *Nature*, 333, 832
- Podsiadlowski, P. 1991, *Nature*, 350, 136
- Podsiadlowski P., Rappaport S., Han Z., 2003, *Mon. Not. R. Astron. Soc.*, 341, 385
- Pols O. R., Schroder K. P., Hurley J. R., Tout C. A., Eggleton P. P., 1998, *Mon. Not. R. Astron. Soc.*, 298, 525

- Podsiadlowski, P., Ivanova, N., Justham, S., Rappaport, S., 2010, *Mon. Not. R. Astron. Soc.*, 406, 840
- Portegies Zwart S. F., Yungelson A., 1998, *A&A*, 372, 173
- Ransom, S. M., et al. 2011, *Astrophys. J.*, 727, 16
- Rappaport, S., Joss, P. C., & Webbink, R. F. 1982, *Astrophys. J.*, 254, 616
- Rasio, F., Pfahl, E. D., & Rappaport, S. 2000, *Astrophys. J.*, 532, L47
- Ray, P. S., et al. 2012, arXiv:1205.3089
- Ricker, P. M., Taam, R., 2008, *Astrophys. J.*, 672, 41
- Ritter, H., & Kolb, U. 2003, *A&A*, 389, 485
- Roberts, M. S. E. 2011, AIP Conference Proceedings of Pulsar Conference 2010 "Radio Pulsars: a key to unlock the secrets of the Universe", Sardinia, October 2010, ed. Burgay, M., D'Amico, N., Esposito, P., Pellizzoni, A., Possenti, A. Roberts, M. S. E. 2012, to appear in IAU Conference Proceedings "Neutron Stars and Pulsars: Challenges and Opportunities after 80 years", ed. van Leeuwen, J., arXiv:1210.6903
- Romanova, M. M., Ustyugova, G. V., Koldoba, A. V., & Lovelace, R. V. E. 2009, *Mon. Not. R. Astron. Soc.*, 399, 1802
- Ruderman, M. A., & Shaham, J. 1985, *Astrophys. J.*, 289, 244
- Ruderman, M. A., Shaham, J., & Tavani, M. 1989, *Astrophys. J.*, 336, 507
- Schatzman, E., 1962, *Ann. Astrophys.*, 25, 18
- Shibazaki, N., Murakami, T., Shaham, T., Nomoto, K., 1989, *Nature*, 342, 656
- Stappers, et al., 1996, *Astrophys. J.*, 465, L119
- Takata, J., Cheng, K. S., & Taam, R. E. 2010, *Astrophys. J.*, 723, 68
- Taam, R. E., & Sandquist, E. L. 2000, *ARA&A*, 38, 111
- Thorstensen, J. R., & Armstrong, E. 2005, *AJ*, 130, 759
- Tout, C. A., Aarseth, S. J., Pols, O. R., & Eggleton, P. P. 1997, *Mon. Not. R. Astron. Soc.*, 291, 732
- Tutukov A., Yungelson L., 1996, *Mon. Not. R. Astron. Soc.*, 280, 1035
- van den Heuvel E. P. J., & van Paradijs, J. 1988, *Nature*, 334, 227
- Verbunt, F., & Zwaan, C. 1981, *A&A*, 100, L7
- Voss R., Tauris T. M., 2003, *Mon. Not. R. Astron. Soc.*, 342, 1169
- Wang, Z., Archibald, A. M., Thorstensen, J. R., Kaspi, V. M., Lorimer, D. R., Stairs, I., & Ransom, S. M. 2009, *Astrophys. J.*, 703, 2017
- Watts, A. L., Krishnan, B., Bildsten, L., & Shutz, B. F. 2008, *Mon. Not. R. Astron. Soc.*, 389, 839
- Webbink R. F., 1984, *Astrophys. J.*, 277, 355
- Willems B., Kolb U., 2002, *Mon. Not. R. Astron. Soc.*, 337, 1004
- Woudt, P. A., Warner, B., & Pretorius, M. L. 2004, *Mon. Not. R. Astron. Soc.*, 351, 1015
- Yungelson L. R., Livio M., Tutukov A. V., Saffer R. A., 1994, *Astrophys. J.*, 420, 336

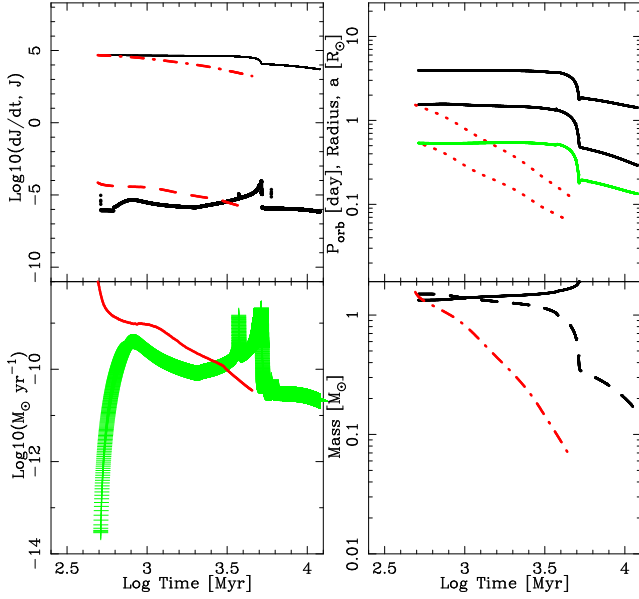


Fig. 1 Comparison between our rapid binary evolution code, BSE, and the detailed stellar evolution code with the inclusion of binary and pulsar evolution. The system begins with $M_1 = 11.83 M_\odot$, $M_2 = 1.64 M_\odot$, $P_{\text{orb}} = 720$ days and zero eccentricity. The mass transfer rate is that given in Hurley, Tout & Pols (2002). The top left panel depicts the evolution of the total change of angular momentum with time (black points) in units of $M_\odot R_\odot^2 \text{yr}^{-2}$ in comparison with that used in the detailed evolutionary model (red dashed line). In units of $M_\odot R_\odot^2 \text{yr}^{-1}$ the orbital angular momentum of both the model presented here (full thin line) and the detailed model (red dash-dot line) are illustrated. In the lower left panel, the mass accretion rate onto the NS (black points, all lie under green pluses) and loss rates from ablation (red points—which are close together) and the companion owing to ‘typical’ mass transfer (green pluses) are illustrated as a function of time. The full red line traces the mass transfer rate from the detailed model. The upper right panel illustrates the orbital separation (top black line) and the companion radius (lower black line) as a function of time. Included is the orbital period in days of our system (green full line) and for comparison the orbital period and radius of the companion from the detailed model (lower and upper dashed red lines respectively). The lower right panel illustrates the variation of the NS mass (solid line) and the companion mass (dashed line) of our model as a function of time compared to the detailed model depicted by the red dash-dot line.

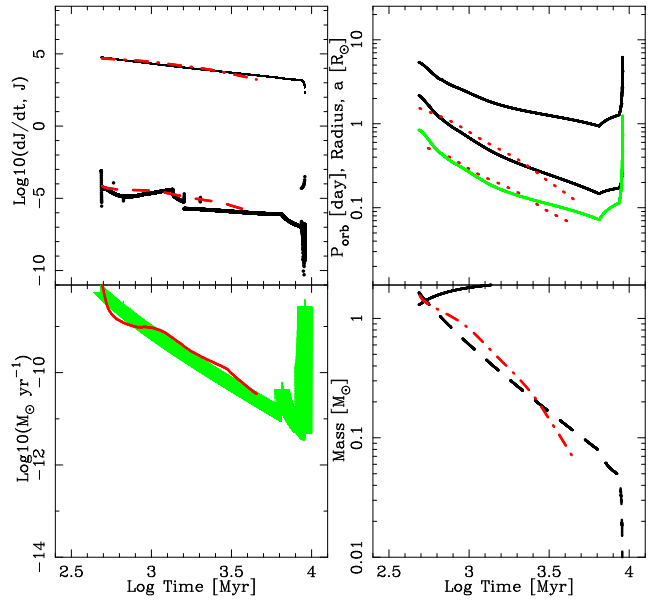


Fig. 2 Comparison between our rapid binary evolution code, BSE, and the detailed stellar evolution code with the inclusion of binary and pulsar evolution. See caption of Fig. 1 for details, however, the mass transfer rate is updated from Hurley, Tout & Pols (2002) equation and is now equation 25.

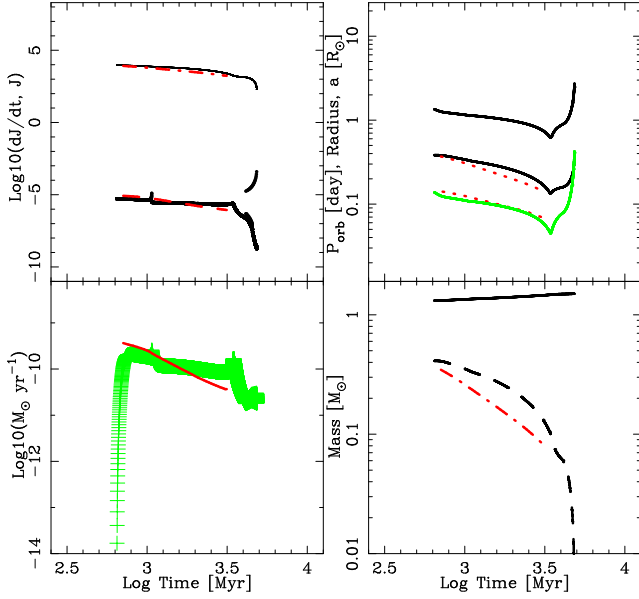


Fig. 3 Comparison between our rapid binary evolution code, BSE, and the detailed stellar evolution code with the inclusion of binary and pulsar evolution. The system begins with $M_1 = 8.936 M_\odot$, $M_2 = 0.4 M_\odot$, $P_{\text{orb}} = 842$ days and zero eccentricity. The mass transfer rate is that given in Hurley, Tout & Pols (2002). The top left panel depicts the evolution of the total change of angular momentum with time (solid black points) in units of $M_\odot R_\odot^2 \text{yr}^{-2}$ in comparison with that used in the detailed evolutionary model (red dashed line). In units of $M_\odot R_\odot^2 \text{yr}^{-1}$ the orbital angular momentum of both the model presented here (full thin line) and the detailed model (red dash-dot line) are illustrated. In the lower left panel, the mass accretion rate onto the NS (black points, all lie under green pluses) and loss rates from ablation (red points—which are close together) and the companion owing to ‘typical’ mass transfer (green pluses) are illustrated as a function of time. The full red line traces the mass transfer rate from the detailed model. The upper right panel illustrates the orbital separation (top black line) and the companion radius (lower black line) as a function of time. Included is the orbital period in days of our system (green full line) and for comparison the orbital period and radius of the companion from the detailed model (lower and upper dashed red lines respectively). The lower right panel illustrates the variation of the NS mass (solid line) and the companion mass (dashed line) of our model as a function of time compared to the detailed model depicted by the red dash-dot line.

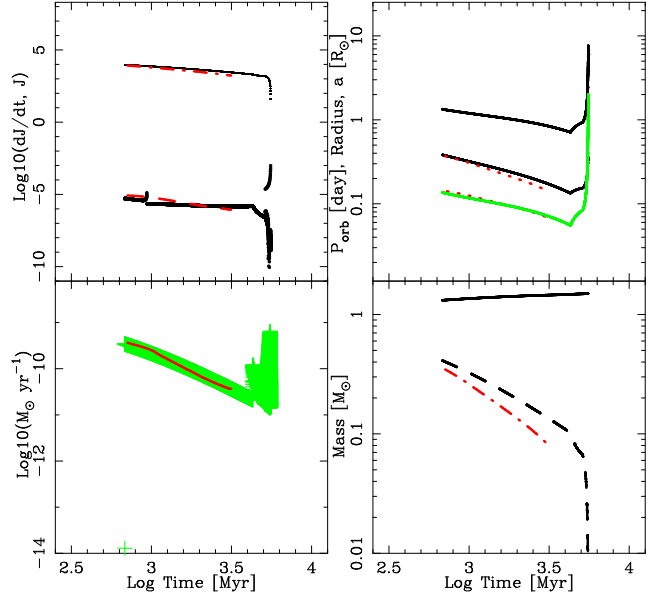


Fig. 4 Comparison between our rapid binary evolution code, BSE, and the detailed stellar evolution code with the inclusion of binary and pulsar evolution. See caption of Fig. 3 for details, however, the mass transfer rate is updated from Hurley, Tout & Pols (2002) equation and is now equation 25.

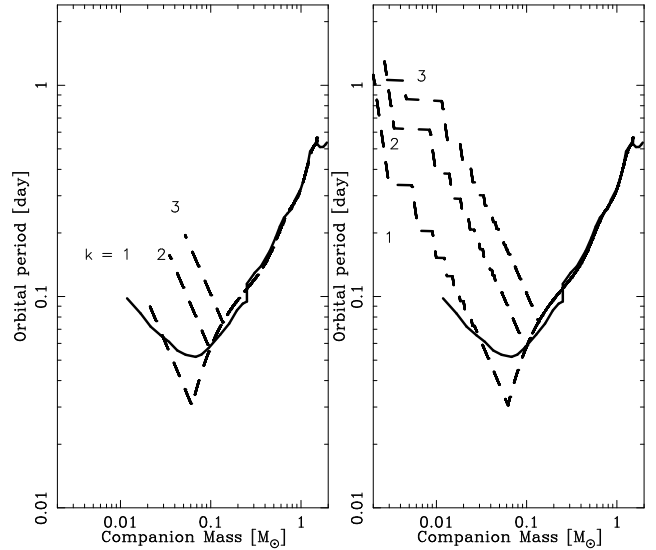


Fig. 5 The evolution from the formation of the NS for the binary evolution based on the population synthesis code and the results from Lin et al. (2011). Direct comparisons in the orbital period versus companion mass are illustrated in both panels. The solid line corresponds to an evolution with a $2 M_\odot$ companion in Lin et al. (2011) as depicted in their fig. 2. The left panel includes models from the population synthesis without ablation or propeller evolution (see dashed lines for $k = 1, 2$ and 3). The right panel corresponds to similar models, but with the ablation and propeller mechanism included assuming $k = 1, 2$ and 3 .

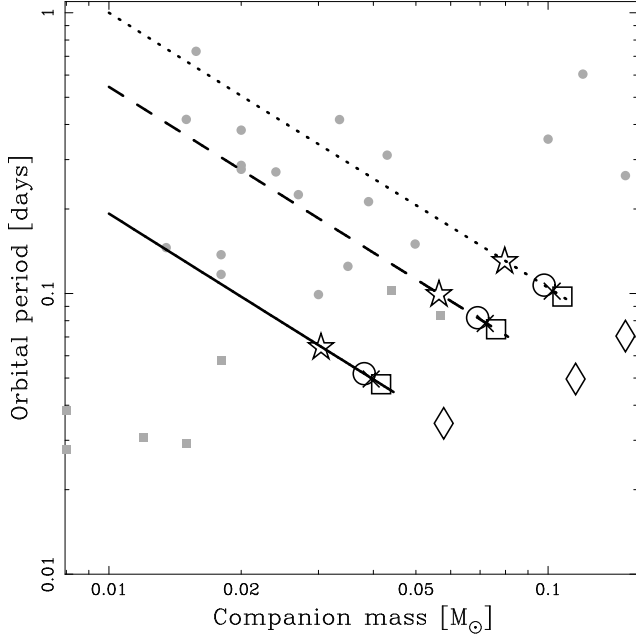


Fig. 6 Typical estimated values of companion mass and orbital period when ablation begins. The sensitivity to model assumptions in determining the transition phase are also depicted. A NS mass of $1.4 M_{\odot}$, eccentricity of zero, pulsar spin period of 5 ms, pulsar magnetic field of 1×10^8 G are adopted. The standard setup is shown with the solid, dashed and dotted lines corresponding to $k = 1, 2$ and 3 respectively. Results are also shown for a NS mass to $2 M_{\odot}$ (cross), pulsar spin period to 1 ms (circle), pulsar magnetic field of 5×10^7 G (square), magnetic field of 10^{10} G (diamond), and a combination of these changes with NS mass $2 M_{\odot}$, spin period of 1 ms and field of 5×10^7 G (star). Each of these assumptions are calculated for each bloating factor. Underlaid beneath the theoretical calculations in grey are observations, with circles representing rotation powered MSPs taken from Table 1 and the ATNF (Manchester et al. 2005) catalogue while squares depict known accretion powered MSPs from the Ritter & Kolb (2003) catalogue. Note that the three highest companion mass systems are not black widow systems but detached MSP-WDs, where the MSP was most likely spun-up by a giant or subgiant star.

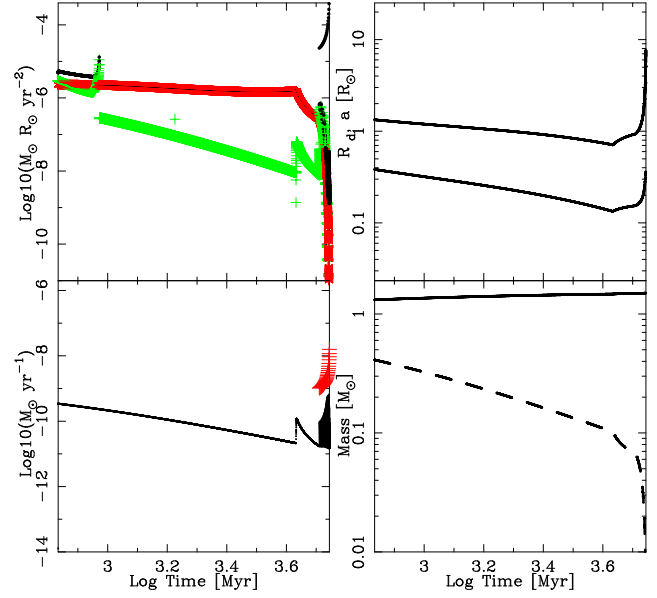


Fig. 7 Detailed evolution of a system initially characterized by $M_1 = 8.936 M_{\odot}$, $M_2 = 0.4 M_{\odot}$, $P_{\text{orb}} = 842$ days and zero eccentricity. The evolution is shown from the onset of RLOF, where we assume that $k = 2$, $f_e = 0.001$ (0.1%) and $f_{\text{eq}} = 0.5$. The top left panel depicts the evolution of the total change of angular momentum with time (black points) and, for comparison, the change in orbital angular momentum owing to tides (green pluses) and gravitational radiation (red asterisk) with time. In the lower left panel, the mass accretion rate onto the NS (black points) and loss rates from ablation (red plus) are shown. The top right panel illustrates the orbital separation (top line) and the companion radius (lower line) as a function of time. The lower right panel illustrates the variation of the NS mass (solid line) and the companion mass (dashed line) as a function of time.

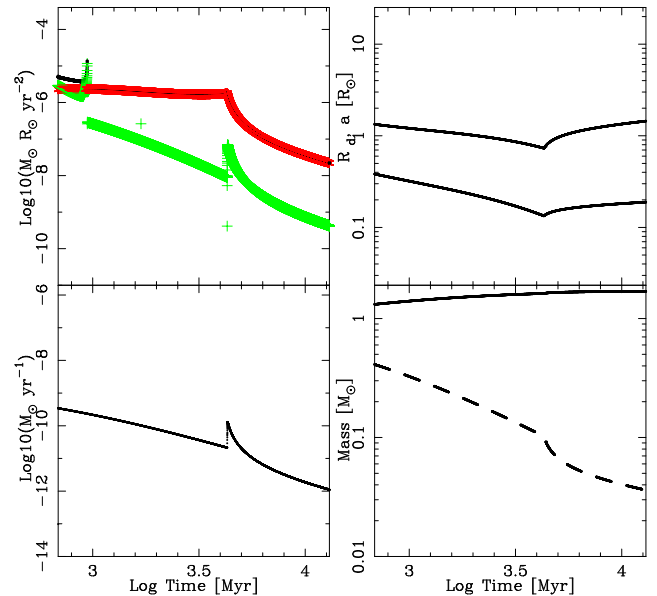


Fig. 8 Except for $M_* = 10^{-6}$, all else follows Fig. 7.

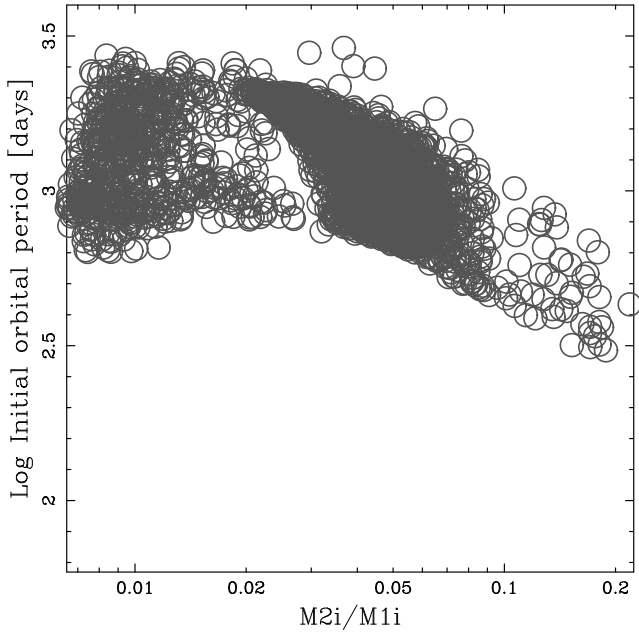


Fig. 9 Initial properties of mass ratio and log of the orbital period are shown for those systems from Model B that are in a black widow system at the end of the simulation.

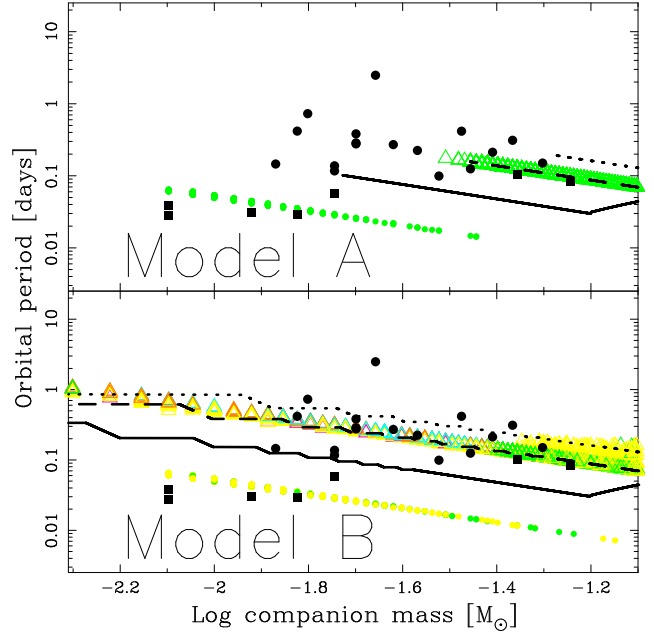


Fig. 10 Orbital period vs companion mass for models A (upper panel) and B (lower panel). Colored triangles represent low mass/semi-degenerate main sequence stars (we simply refer to these as MS-MSP systems), while colored dots represent He/CO/ONe WDs (which we refer to as WD-MSPs). The different colors denote different phases of evolution; RLOF is green, mass transfer during spin equilibrium evolution is yellow, ablation while on the equilibrium line is magenta, ablation during propeller evolution is cyan and the detached phase is orange. Over plotted on both panels are black points depicting observed systems. Full squares are X-ray binaries with known accretion powered MSPs taken from the Ritter & Kolb (2003) catalogue. Full circles are known black widow pulsars taken from Table 1 and making use of the ATNF catalogue (Manchester et al. 2005) assuming $M_{\text{NS}} = 1.35$ and $i = 60^\circ$. The lines represent a particular system from the same model but with $k = 1$ (full line), $k = 2$ (dashed line) and $k = 3$ (dotted line). The system begins with $M_1 = 8.936 M_\odot$, $M_2 = 0.4 M_\odot$, $P_{\text{orb}} = 842$ days and zero eccentricity.

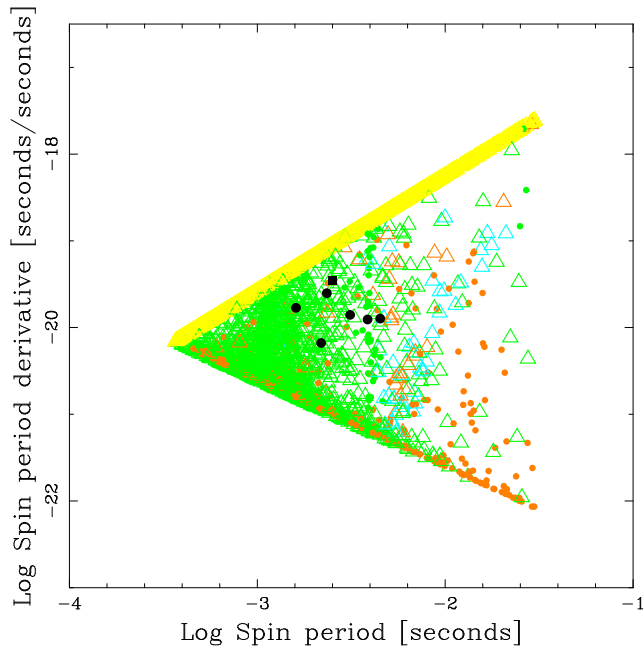


Fig. 11 The spin period-spin period derivative of our model B systems depicted in Fig. 10. The model points and colors are those of Fig. 10, model B, where we $k = 2$, $f_e = 0.001$ (0.1%) and $f_{\text{eq}} = 0.5$. Overlaid on our model are six black widow pulsars with known \dot{P} . The black square is J1808 (Watts et al. 2008).

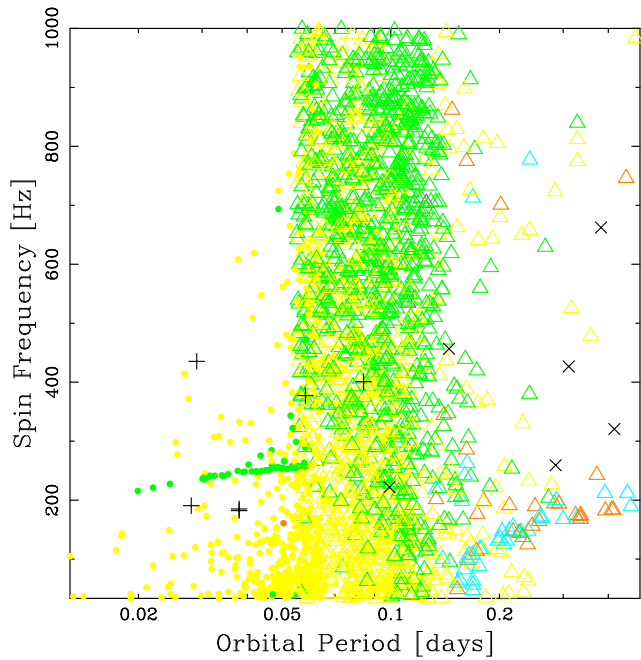


Fig. 12 Spin frequency vs. orbital period, comparing the results of systems from model B (colors and symbols as in Fig. 10) to observations of accretion powered MSPs (plus symbols) and rotation powered MSPs (cross symbols).